Check for updates

Effect of gamma irradiation on the electrical and optical properties of PEVA composite membrane embedded with conductive copper fluoroborate glass powder

Elbadawy A. Kamoun, [ID] *[ab] O. I. Sallam,[c] Ehab E. Khozemy,[c] Mohamed Morsy,[de] Yasair Al-Faiyz, [ID] [a] Saleh M. Matar,[fg] Ahmed I. Ali, [ID] *[hi] Jong Yeog Son [ID] *[i] and Galal H. Ramzy[j]

A series of thin films of poly (ethylene-*co*-vinyl acetate) (PEVA) mixed with different amounts of conductive fluoroborate glass powder doped with copper oxide particles (0, 0.2, 0.4, 0.6, 0.8, 1, 1.3 and 1.5 wt%) were prepared *via* a melt-quenching technique. The effect of irradiation dose exposure up to 40 kGy was investigated at room temperature in the air. Meanwhile, the homogeneity of glass powder dispersion on the PEVA matrix was studied based on the crystallinity of the composite sheets and morphology using X-ray diffraction (XRD). Field-emission scanning electron microscopy (FE-SEM) revealed that the homogeneous distribution of CuO nanoparticles through the entire polymer matrix was the main feature of the polymer-reinforced samples. In addition to dielectric properties, frequency and temperature dependencies were studied. Further, the thermal stability of the composite sheets was investigated. Optical studies revealed that the bandgap energy and content of conductive glass decreased with radiation. The conductivity of the composites $\sigma_{AC}(f)$ was evaluated according to Jonscher's universal power law. Further, the addition of conductive glass to the PEVA improved the thermal stability of the composites (20 °C to 80 °C), as measured experimentally. The conductive glass additive enhanced the structural, morphological, optical, thermal, and electrical properties of PEVA for industrial applications.

a Department of Chemistry, College of Science, King Faisal University, Al-Ahsa 31982, Saudi Arabia. E-mail: ekamoun@kfu.edu.sa

b Polymeric Materials Research Department, Advanced Technology and New Materials Research Institute (ATNMRI), City of Scientific Research and Technological Applications (SRTA-City) Alexandria, New Borg El-Arab City, Egypt

c Radiation Chemistry Department, National Center for Radiation Research and Technology, Egyptian Atomic Energy Authority (EAEA), P.O. Box 8029 Ahmed El-Zomr, Cairo 11371, Egypt

d Nanotechnology Research Center (NTRC), The British University in Egypt (BUE), El Sherouk City, Suez Desert Road, Cairo 11837, Egypt

e Building Physics and Environment Institute, Housing & Building National Research Center (HBRC), 12311 Dokki, Giza, Egypt

f Chemical Engineering Department, Faculty of Engineering, Jazan University, Jazan 45142, Saudi Arabia

g Bioprocess Development Department, Genetic Engineering and Biotechnology Research Institute (GEBRI) City of Scientific Research and Technological Applications (SRTA-City), New Borg Al-Arab City 21934, Alexandria, Egypt

h Basic Science Department, Faculty of Technology and Education, Helwan University, Saray–El Qoupa, El Sawah Street, 11281 Cairo, Egypt. E-mail: Ahmed_Ali_2010@techedu.helwan.edu.eg

i Department of Applied Physics and Institute of Natural Sciences, College of Applied Science, Kyung Hee University, Suwon 446—701, Republic of Korea. E-mail: jyson@khu.ac.kr

j Physics department, Faculty of Science, Cairo University, Giza 12613, Cairo, Egypt

1. Introduction

Recently, the industry has increased the application of polymeric materials with electrical conductive properties. Therefore, research and development (R&D) is required, especially for properties such as elastic, electrical, and optical properties. Because of their high tensile strength, ease of preparation, low cost, and flexibility, polymers are good candidates for many industrial applications.[1–3]

Conductive polymer-glass composite films have gained great attention owing to their excellent dimensional stability, safety, manufacturing simplicity, electrochemical characteristics, and processability.[4–6] However, the use of polymer sheets faces some limitations as they have low ionic conductivity. Low ionic conductivity in polymers originates from the ionic transport mechanism, which depends on the movement of ions within the polymer due to additives such as lithium ions[4] that lead to local relaxation of the movement of polymeric chains. Solid polymer electrolytes with inorganic additives are used in polymers to improve not only electrical properties but also mechanical properties and thermal stability.[7]

Many studies have been carried out to enhance the optical and electrical properties of polymers by doping inorganic

oxides, which enhance dielectric properties. Inorganic additives were used with polymers not only to improve electrical properties but also to improve mechanical properties and increase thermal stability.[8] The electrical conductivity of many polymers including polyethylene glycol (PEG),[9] polyvinyl pyrrolidone (PVP),[10] polyvinyl chloride (PVC),[11] and polyvinyl alcohol (PVA)[12] has been improved by the addition of inorganic metal oxides such as copper, titanium, aluminum, and lithium.[13,14] In our previous research work, polyelectrolyte membranes based on phosphorylated-PVA/cellulose acetate were investigated for direct methanol fuel cell applications[15] by doping oxidized cellulose with $Bi_{0.5}Na_{0.25}K_{0.25}TiO_3$ films fabricated for optoelectronic application.[16] Further, novel glass material-based (PVA/PVP/Al_2O_3/SiO_2) hybrid composite hydrogel membranes have been synthesized for industrial applications.[17]

Polyethylene vinyl acetate (PEVA) has excellent properties including a low melting point, resistance to UV radiation, and good clarity and gloss due to which it is competitive with rubber in many electrical applications.[18] Moreover, PEVA has high electrochemical stability, high flexibility, excellent tensile strength, and compatibility with inorganic oxides and carbonaceous materials that can be used in the production of conductive sheets and thin transparent films easily without plasticizers or laxative additives.[19–21]

Ionizing radiation is used as a green method for obtaining new materials with excellent properties.[22] However, this can lead to changes in polymer properties as the radiation can break bonds and form free radicals to create new bonds with the reactants, thus imparting unique qualities to conventional polymers.[23] These characteristics depend on the materials used and irradiation dose. Incorporating semiconductor glass as a filler in polymer membranes improves three-dimensional stability and thus enhances mechanical strength. The effects of doping CuO, CoO, Fe_2O_3, and NiO in $20NaF–60P_2O_5–20Na_2O$ on its dielectric properties were investigated, and the results indicated improved ac conductivity and increased charge carrier motion caused by an increase in polaron hopping of ions between their valence states.[24]

Glasses are highly three-dimensional disordered structures containing varied-sized tunnels that form a network. Small-sized cations like lithium ions are preferred for improving the electrical conductivity of glasses, whereas large-sized cations are not suitable for this purpose because they can block the tunnels.[25] Boron oxide is a known dopant used in borate glasses, which are famous next to silicate glasses. Borate glass is different from silicate glasses since the former has two structural units, namely triangular [BO_3] and tetrahedral [BO_4] units,[26] while silicate glass has only one tetrahedron [SiO_4] structural unit.[27] When alkaline/alkali oxides are incorporated in borate glass units, the $BO_3 \leftrightarrow BO_4$ conversion process occurs, and changes in physical properties are observed.[28]

Moreover, alkali fluorides, such as LiF, can eliminate –OH groups from the borate network structure to give a 3-D network and cause BO_3 and BO_4 to be converted into $BO2F$ and $BO3F$ units,[29] thus endowing new structural and physical properties to borate glasses. Hence, lithium ions add good electrical properties to fluoroborate glasses because the smaller size of

Li^+ ions allows them to hop easily through the tunnels inside the glass network and enhance the movement of charges, thus enabling the glass systems to be used in solar energy converters, electrochemical devices and energy batteries.[26] However, when transition metals (*e.g.* copper oxide) are added to the fluoroborate network, the semiconductor characteristics can be obtained.[30] Due to the unique hopping mechanism related to the different electronic valences of transition metals, copper ions can exist in the glassy matrix as metallic copper Cu°, cuprous Cu^+ or/and cupric Cu^{2+} with the electronic structure ($3d^{10}$ $4s^1$). Color centers can be created as Cu^{2+} ions can give blue glass; however, if a majority of copper ions exist as Cu^+ rather than Cu^{2+}, the glass will appear green.[31] The hopping mechanism involves the hopping of electrons between valences and being trapped by positive-charged holes as electrons of lower valence (Cu^+) move into higher valences (Cu^{2+}) and combine with optical phonons.[32] Cu^+ exhibits broad bands in optical studies due to the coupling of s-electrons and phonons besides the s → d transition.[33]

In this study, copper fluoroborate glass powder was prepared by a facile method through a melting-quench technique and loaded as a conductive filler in the PEVA polymeric membrane. The effects of gamma irradiation on the structural, optical, and electrical properties of the prepared composite films were intensively investigated. The results show that the resultant properties entirely depend on the internal hopping of lithium ions and the changes in the valence of the copper ions. The gamma irradiation enhanced the physical properties of the prepared composite films, rendering them suitable for conducting polymer applications in electronic devices.

2. Materials and methods

2.1. Materials

For the polymer membrane, ethylene vinyl acetate (PEVA) (melt flow index 19 g for 10 min, melting point of 67 °C, containing 18% vinyl acetate) was supplied by Arkema Inc., North America, Colombes, France. The structure of PEVA is shown in Scheme 1. The raw materials used for glass preparation, including boric acid (H_3BO_3), cadmium carbonate ($CdCO_3$), sodium carbonate (Na_2CO_3), sodium fluoride (NaF) and copper oxide (CuO), were of commercial grade and were purchased from Sigma Aldrich, Germany.

2.2. Gamma irradiation facility

Gamma irradiation of the samples was carried out using the ^{60}Co source in the gamma chamber-4000A installed at the National Center for Radiation Research and Technology,
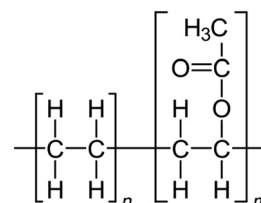
Scheme 1 Chemical structure of PEVA.[34]

Egyptian Atomic Energy Authority, Cairo, Egypt. It was manufactured by the Atomic Research Center in Bombay, India. The compounds were subjected to gamma irradiation in the air at room temperature. The irradiation was carried out at a dose rate of 1.3 kGy h^{-1}.

2.3. Preparation of the glass samples

A homogenous mixture of 60 mol% B_2O_5, 10 mol% CdO, 15 mol% Na_2O and 15 mol% NaF was doped with 5% CuO. The raw materials were mixed and melted in a porcelain crucible at 1100 °C in an electrical furnace for 1 h. The molten sample was then poured on a hot pure stainless-steel mold to quench the sample. The resulting sample was placed in an annealing furnace quickly, annealed at 300 °C for 1 h and left to cool down naturally till it reached room temperature. The obtained sample was crushed into chunks and ground by ball milling to a fine powder with a particle size of about 45 μm.

2.4. Preparation of the PEVA composite membrane

Polyethylene vinyl acetate was melted in a hot mixer twin-screw operated at a speed of 80 rpm at 120 °C for 5 minutes. The conductive glass powder prepared was added at different proportions and mixed for 15 minutes until complete homogeneity of the composite mixture was achieved. The mixing process was carried out without laxatives. Different amounts (0, 0.2, 0.4, 0.6, 0.8, 1, 1.3 and 1.5 wt%) of the prepared conductive powder glass were used for the production of composite membranes, as shown in Table 1. The mixed composite samples were pressed to form sheets by using a Carver hydraulic hot press at 110 °C and a pressure of 160 kg cm^{-2} for at least 5 minutes on the mold surfaces. The prepared composite sheets were subjected to ^{60}Co-gamma rays at an irradiation dose of 50 kGy at a dose rate of ≈ 1.3 kGy h^{-1}.

2.5. Characterization techniques

The X-ray diffraction (XRD) patterns of all prepared samples were acquired using an Empyrean 3 diffractometer from Malvern Panalytical, France. The phase structure of the samples was analyzed by XRD data obtained on a Bruker D8 Advance diffractometer with Copper K radiation (radiation wavelength = 1.54056 nm) operated at 40 kV and 40 mA. The sample was scanned in the 2θ range of 10–60° in the step-scan mode (0.02° per step).

The morphology and chemical compositions of the prepared membranes were investigated by field-emission electron

microscopy (FE-SEM) (Model-Quanta FEI200, FE-SEM, Thermo-Scientific, USA). FT-IR spectra were recorded in the spectral range of 4000–400 cm^{-1} using a Vertex 70 (Cary series, Bruker, Germany). The optical properties of the samples were measured by UV/visible spectroscopy (Cary series UV/vis, Bruker, Germany). Absorption and transmittance values were recorded in the wavelength range of 300 nm to 800 nm. The optical parameters were estimated using known empirical equations. The dielectric characteristics were measured as functions of frequency at room temperature using an LCR meter (Haioki 3533, Japan) in the range of 100–200 kHz at a potential difference of 1 mV.

3. Results and discussion

3.1. X-Ray diffraction

The XRD patterns of all the samples before and after irradiation are indicated in Fig. 1(a and b), respectively. The samples were measured from 2θ = 10° to 60° with a step size of 0.2°. The diffraction patterns demonstrate two peaks at 2θ 21.3° and 23.5°, which can be attributed to the diffraction planes (110) and (200) related to the PEVA polymer, respectively.[1] The characteristic peaks of the PEVA polymer were identified in all the prepared samples. Meanwhile, for oxide-included oxide materials, no diffraction peaks were observed due to the amorphous nature of the oxide-incorporated glass powder. No other diffraction peaks belonging to impurities or foreign materials were observed, confirming the purity of the cast membrane samples.

For the irradiated samples, the XRD patterns demonstrated a crystalline structure, with diffraction peaks at 2θ = 21.3° and 23.5° corresponding to the (110) and (200) diffraction planes, respectively. Moreover, the irradiated samples exhibited more intense peaks than the non-irradiated samples. The intensity increment might be directly related to the crystallinity of the prepared materials.[1] An additional feature related to the noise level was observed, with the irradiated samples showing less noise than the non-irradiated samples (Fig. 1a and b).

3.2. FT-IR spectroscopy

The chemical bonding formed between the constituents of the synthesized structures was confirmed through FT-IR measurements. The FT-IR absorbance spectra were recorded in the spectral range from 4500 up to 400 cm^{-1}, as depicted in Fig. 1(c and d). The band assignments are tabulated in Table 2. The FT-IR analysis characterized the presence of absorbance bands in the frequency range lower than 1000 cm^{-1}, confirming the presence of metal oxide ions.

Moreover, the bands assigned to the PEVA polymer agree with previously published reports.[2–7] The peak intensity did not change as the amount of the dopant increased. This can be due to the good dispersion and distribution of the dopant inside the PEVA matrix.

3.3. FE-SEM investigation and EDX analysis

The SEM images of all samples were observed to investigate the morphological features of the samples and trace the distribution of the incorporated glass powder in the matrix of the PEVA

Table 1 Formulations of PEVA composite membranes embedded with the copper fluoroborate conductive glass powder

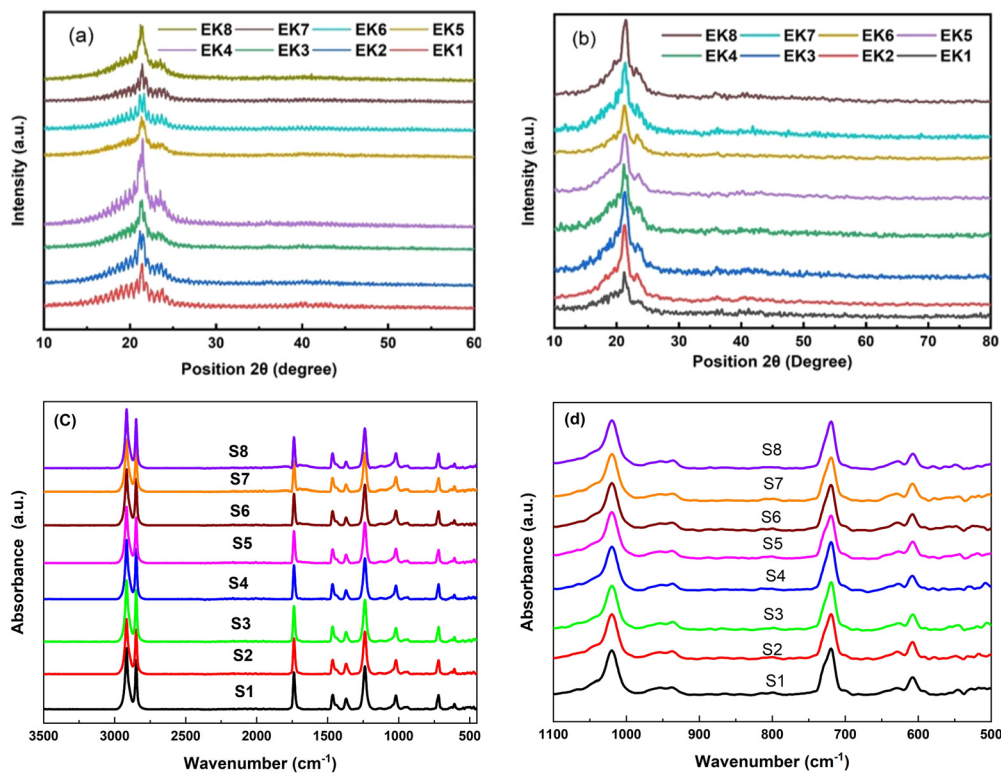| Sample code		PEVA (g)	Glass powder (wt%)
S1	EK1	100	0.0
S2	EK2	99.8	0.2
S3	EK3	99.6	0.4
S4	EK4	99.4	0.6
S5	EK5	99.2	0.8
S6	EK6	99.0	1
S7	EK7	98.7	1.3
S8	EK8	98.5	1.5

Fig. 1 XRD patterns of the PEVA composites (a) before and (b) after irradiation. (c) FT-IR spectra and (d) magnified IR spectra at lower wavenumbers (500–1100 cm^{-1}) of PEVA mixed with different amounts of conductive ground glass particles (0, 0.2, 0.4, 0.6, 0.8, 1, 1.3 and 1.5 wt%).

Table 2 FT-IR band assignment of PEVA samples mixed with different amounts of conductive ground glass powder particles (0, 0.2, 0.4, 0.6, 0.8, 1, 1.3 and 1.5 wt%)

Wavenumber (cm^{-1})	Functional group	Type of vibration
2916	$-CH_2-$	Antisymmetric stretching
2845	$-CH_2-$	Symmetric stretching
1738	C=O easter	Stretching
1468	$-CH_2-$	Deformation in the plane
1369	$-CH_3-$	Deformation in the plane
1237	C–O	Antisymmetric stretching
1023	=C–O–C	Symmetric stretching
721	$-CH_2-$	Inner rocking vibration of CH_2 in the amorphous part

polymer. The surface morphology of the sample without the glass was also captured at the same magnification for comparison. The elemental composition was confirmed by EDX, which is an effective tool for quantifying the ratio of constituents. The SEM images of all the prepared samples are shown in Fig. 2. The SEM micrograph of the glass sample (Fig. 2a) displayed sharp-edged fragments with irregular shapes and varied sizes. Moreover, the SEM images in Fig. 2b to g represent the PEVA polymer containing different ratios of glass fragments. The EK1 sample displayed a smooth background, which represented the polymer matrix, while CuO was seen as white dots on the background. The main feature of the polymer-reinforced sample was that the CuO nanoparticles were distributed homogeneously in the entire polymer matrix. In the EK2-EK8 samples, two distinct components (CuO and glass particles) were apparent. The difference in size between the CuO and glass

fragments could be distinguished. As the ratio of glass increased, the amount of white dots representing the glass fragments increased by 1%. Further increment in the glass fragment ratio resulted in agglomeration, as seen clearly in Fig. 2h and i.

The elemental analysis was performed to confirm (quantitatively and qualitatively) the elemental composition of the prepared samples, as shown in Fig. 3. The EDX spectrum of the EK0 sample (Fig. 3a) displayed Cd, Ba, Na, Cu, and F as the constituent elements of the incorporated glass powder. The EDX spectrum of the EK1 sample, which contains PEVA polymer and copper oxide (Fig. 3b), demonstrated the presence of carbon, oxygen, and copper as the elementary components. The amount of glass increased from 0% in EK1 to 1.5% in the EK8 sample. EK3, EK6, and EK8 samples were selected to confirm the dispersion of glass inside the polymer matrix.
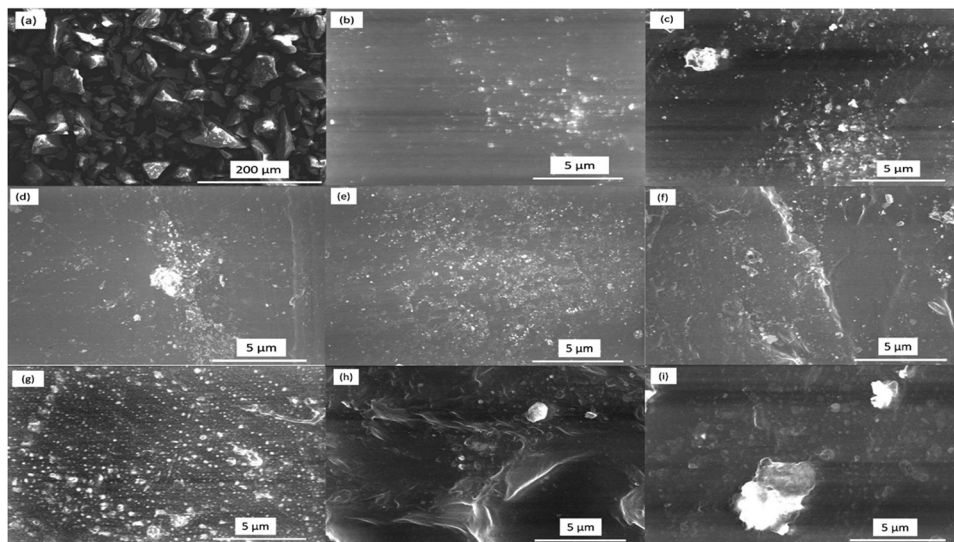
Fig. 2 FE–SEM images of PEVA samples mixed with different amounts of conductive ground glass powder particles (0, 0.2, 0.4, 0.6, 0.8, 1, 1.3 and 1.5 wt%): (a) glass only, (b) EK1, (c) EK2, (d) EK3, (e) EK4, (f) EK5, (g) EK6, (h) EK7, and (i) EK8.

As shown in the EDX analysis of the membrane samples coded EK3, EK6, and EK8, the constituent elements of glass, including Cd, Ba, Na, Cu, F, O, and C, were well-dispersed inside the PEVA polymer matrix (Fig. 3c, d and e, respectively). Moreover, the peaks of glass-forming elements increased as the amount of dispersed glass increased. The EDX analysis demonstrates the inclusion of varied amounts of glass powder inside the PEVA polymer matrix.

3.4. Optical properties

Fig. 4 presents the optical properties of the polyethylene vinyl acetate (PEVA) composite with a glass composition of 60% B_2O_3 + 10% CdO + 15% Na_2O + 15% NaF doped with 5% CuO before and after irradiation. Fig. 4(a) and (c) are the UV/vis spectra showing the transmission-wavelength dependences of the composites before and after irradiation. At lower wavelengths, $\lambda <$ 250 nm, the transmission of the irradiated samples was independent of the concentration of the incorporated glass powder but started to increase at $\lambda > 250$ nm. However, after irradiation of the samples, their transmission started to increase at $\lambda > 300$ nm, and the starting point of the irradiated samples moved to higher wavelengths. On comparing the transmittance (%T) of the samples before and after irradiation, as shown in Fig. 4(a) and (c), the value of %T was found to decrease with radiation. In addition, %T increased with doping up to 6% of incorporated glass powder and decreased with a further increase in doping level. Furthermore, the reflections of the samples before and after irradiation were similar, as shown in Fig. 4(b) and (d), and the only difference was that they had shifted from 250 nm to higher wavelengths ($\sim$350 nm). From the experimental optical absorption data, it is expected that the energy bandgap changes due to the irradiation of the samples as it affects the transmission and absorption data. Thus, the photon of radiation energy might excite electrons from the valence band to conduction band.

Using the spectra of (R) and (T), the absorption coefficients (α) of the samples under study were calculated using the following equation.[35]

$$\alpha = \left(\frac{1}{d}\right) \ln\left(\frac{(1-R^2)}{T}\right) \tag{1}$$

where (d) is the film thickness. The optical energy gap (E_g) was determined using the following equation.

$$\alpha = A(h\nu - E_g)^p \tag{2}$$

The relationship between ($\alpha \cdot h\nu)^2$ and ($h\nu$) is shown in Fig. 5(a and b). The plots show that the optical bandgap energy increased with the glass content up to $x = 0.4$ and decreased with the addition of more glass due to the accumulation of Cu ions on the surface of the composites. Compared with the irradiated samples, the bandgap energy E_g for the virgin polymer sample (PEVA) decreased from 4.12 eV to 3.85 eV. However, all other samples were influenced by the radiation, as shown in Table (3).

The radiation decreased the bandgap energy of the composites of the PEVA polymer matrix. The general trend of band gap energies with conductive glass doping in the PEVA polymer was a linear decrease, as listed in Table 3. This is expected because the photon energy of radiation can excite the electrons from the valence band to the conduction band. The effect of radiation on the polymers is correlated with network formation and the incorporation of cross-linked segments into the crystalline phase during the recrystallization process.[36]

Fig. 6(a and b) present the refractive index and extinction coefficient spectra of all prepared samples. The refractive indexes (n) of these samples were calculated using the following equation.[37]

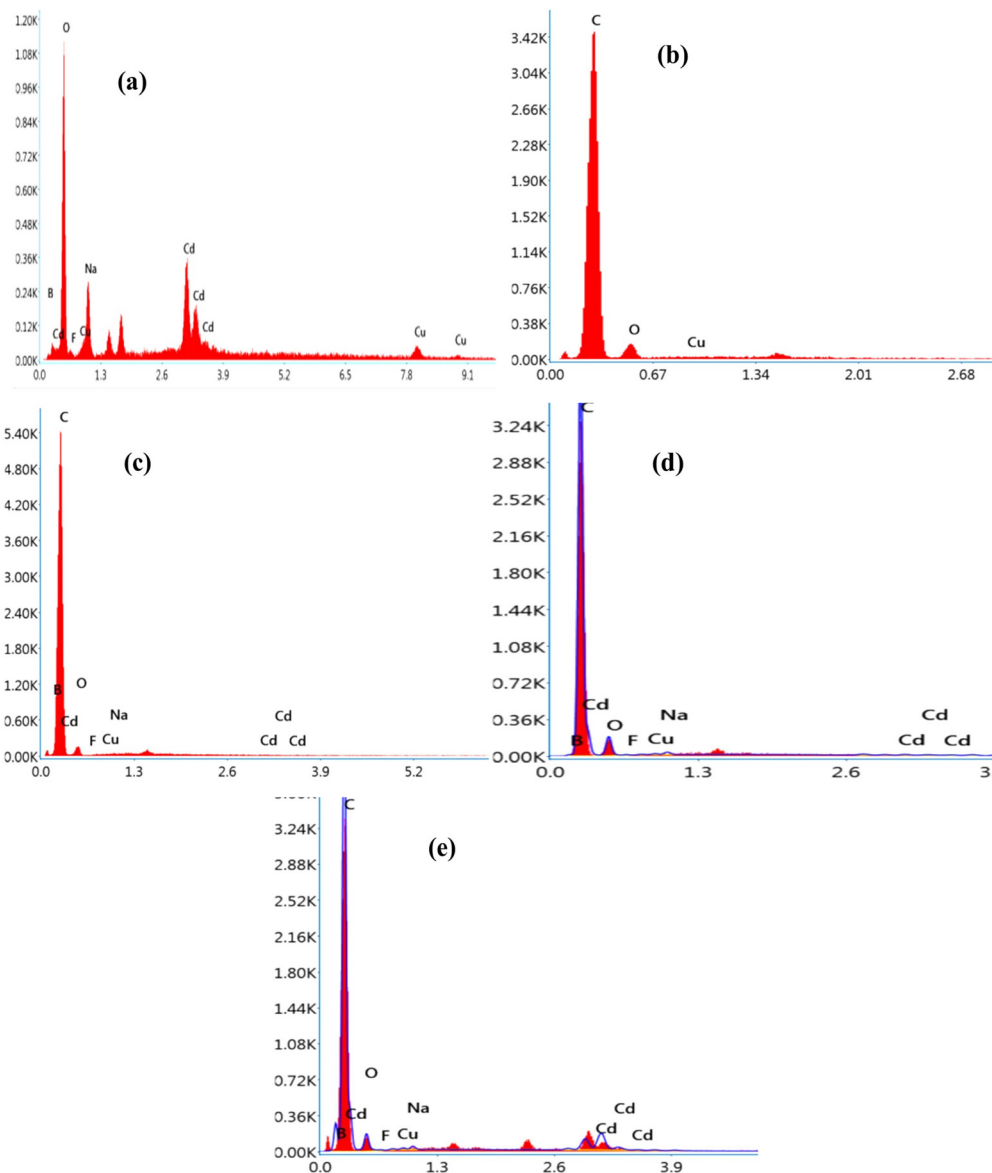$$n = \left(\frac{(1+\sqrt{R})}{(1-\sqrt{R})}\right) \tag{3}$$

Fig. 3 EDX analysis of selected PEVA composite membranes containing different amounts of conductive ground glass powder particles (0, 0.2, 0.4, 0.6, 0.8, 1, 1.3 and 1.5 wt%): (a) EK0, (b) EK1, (c) EK3, (d) EK6, and (e) EK8.

The influence of photon energy on (n) of the prepared samples is shown in Fig. 6(a). The refractive index (n) increased with the glass content owing to the increase in (R) values. It could be observed that the n-values increased at low energy values $E_g < 3$ eV, while at high energy values (photon energy > 3.5 eV), the refractive index decreased, and this might be due to the breakdown of the dielectric of the PEVA polymer matrix at high energies.

It is known that radiation can induce crosslinking in a polymer matrix. The interaction of the glass components with the Cu element may influence the nature of the reactions in the matrix. Therefore, the copper element might serve as a cross-linking agent, leading to a more cross-linked and stable polymer structure. The polymer undergoes excitation and ionizes because the polymer can absorb radiation, which in turn, can produce the initial chemical reactants.[38]

The extinction coefficient, (k), which is dependent on the imaginary part of the refractive index and describes the ability of the samples to absorb light, was determined using the below equation:[39]

$$k = \alpha \cdot \frac{\lambda}{4\pi} \tag{4}$$

The extinction coefficient (k) of the PEVA/glass powder composition (60% B_2O_3 − 10% CdO − 15% Na_2O − 15% NaF doped with 5% CuO) before and after irradiation is presented as a function of the photon energy in Fig. 6(b and d), respectively. The results show that the effect of radiation clearly as the k-values increased from 2000 to 4000 with radiation. This means that the irradiated composite samples absorbed photon energy better than the virgin samples. Moreover, their k-values
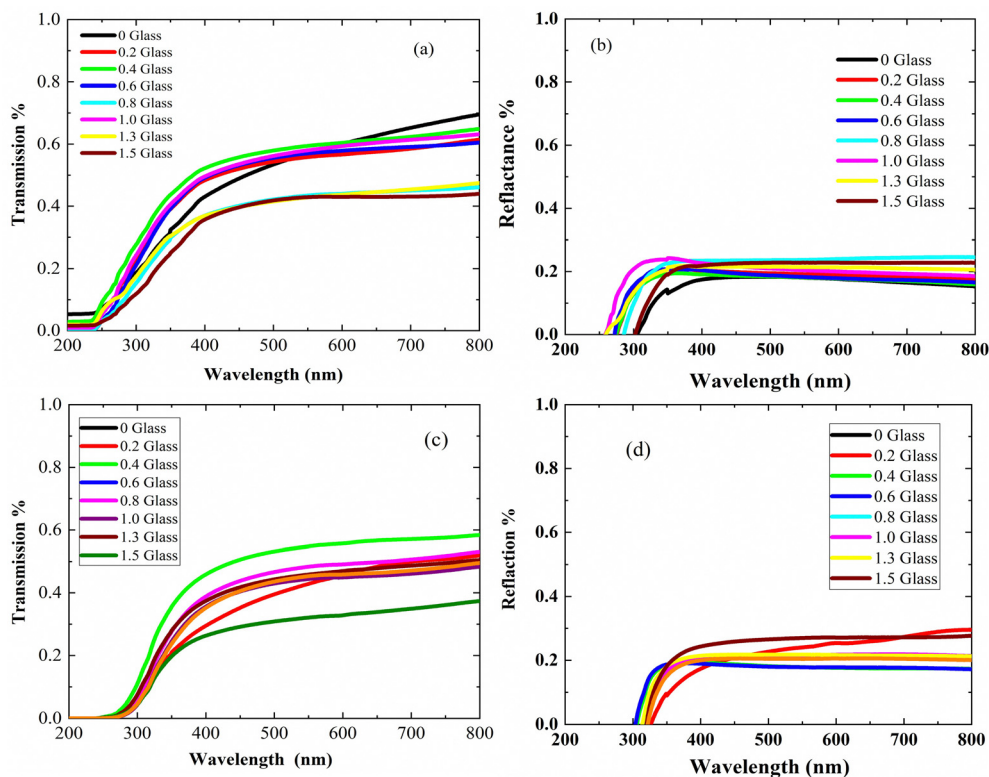
Fig. 4 Optical properties of glass–powder–incorporated PEVA composite membranes with the composition 60% B_2O_3 + 10% CdO + 15% Na_2O + 15% NaF doped with 5% CuO: (a) transmission and (b) reflection before irradiation; (c) transmission and (d) reflection after irradiation.
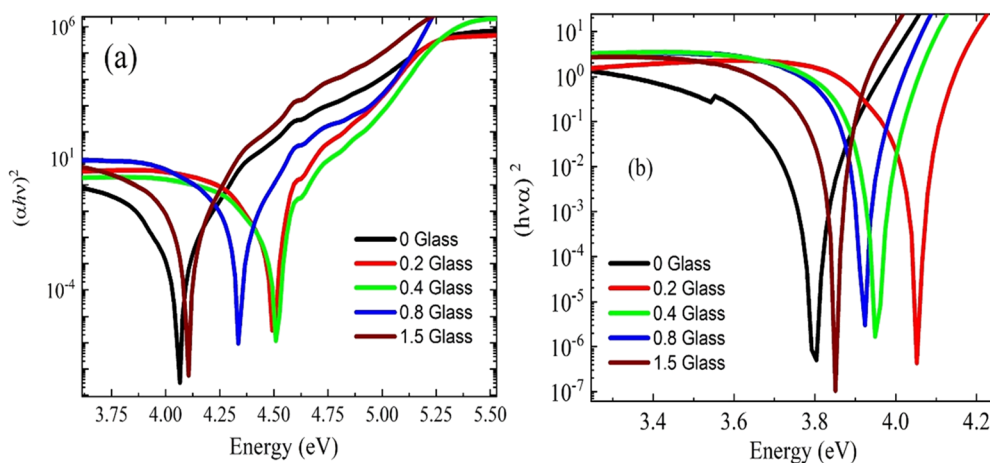

Fig. 5 Optical bandgap energies of the prepared PEVA/glass powder composite membranes with the composition 60% B_2O_3 ± 10% CdO + 15% Na_2O + 15% NaF doped with 5% CuO: (a) before irradiation and (b) after irradiation.

increased at a photon energy (4.5 eV) lower than the version samples (5 eV).

Previous studies on γ-irradiated polymers have revealed a shift toward lower energies and that radiation has a considerable effect on the optical bandgap energy, showing a decrease from 4.20 to 3.96 eV because of indirect allowed transitions. Moreover, the refractive indices of the polymer samples were considerably high, and the values increased with the effect of gamma dose.[40–45]

3.5. Dielectric properties

3.5.1. Dielectric properties as functions of frequency. The experimental dielectric data is considered a powerful tool to explore the dynamic properties of a composite, such as the real part of the dielectric constant (ε'), the imaginary part of the dielectric constant (ε''), and AC conductivity (σ_{AC}).[46,47] One of the most important advantages of frequency-dependent dielectric properties data is the information about the contributions

Table 3 Band gap energies of (PEVA) mixed with different amounts of conductive ground glass particles (0, 0.2, 0.4, 0.6, 0.8, 1, 1.3 and 1.5 wt%) before and after exposure to radiation

Sample codes		Glass powder (wt%)	E_g (eV) unirradiated	E_g (eV) irradiated
S1	EK1	0.0	4.065	3.8
S2	EK2	0.2	4.49	4.6
S3	EK3	0.4	4.51	3.94
S5	EK5	0.8	4.34	3.92
S8	EK8	1.6	4.1	3.85

of different factors, including grain boundaries, bulk material, and electrode effects.[48]

The complex dielectric constant and dielectric loss of a material are defined as:[49,50]

$$\varepsilon^* = \varepsilon' - i\varepsilon'' \tag{5}$$

where ε' and ε'' are the real part and imaginary part of the complex dielectric constant, respectively.

The real part of the dielectric constant (ε') represents the energy stored inside the dielectric sample between the conductive electrodes. However, the imaginary part of the dielectric constant (ε'') reflects the energy loss in the dielectric sample. Because of a sample exhibits energy loss under an applied electric field at front of the polarization, resulting in the grain boundaries.[51] Further, the loss takes place due to three factors, including dipole loss or molecular dipole movement, space charge migration, and direct current conduction.[52]

Fig. 7 presents the ε', ε'' and AC conductivity (σ_{AC}) *versus* frequency (f) at a constant temperature of 40 °C. The ε'–values of PEVA with conducting glass powder at 40 °C decrease with increasing frequency up to ($f < 1$ kHz), while it remains constant at higher frequencies ($f > 1$ kHz). The effect of irradiation on the membrane samples is very clear since the irradiated samples exhibit dielectric breakdown except for the composite with 0.4 content of conductive glass (S3:0.4), which showed different behaviour from all the other samples. Moreover, the ε' values of the samples increased from around 30 up to 1000 due to the effect of radiation.

In the ε' against f plots (Fig. 7(a)), ε' deceased with increasing frequency and its value become constant at high frequencies. A similar behavior was observed for ε'' against f (Fig. 7(b)). On the other hand, the electric conductivity (σ_{AC}) increased with the frequency (Fig. 7(c)). The large values of ε' and ε'' in the low-frequency range arise due to increased charge polarization at the electrode interface due to Li$^+$ ions, adding to the low conductivity at the grain boundaries.[50,53] Moreover, the $\sigma_{AC}(f)$ can be expressed according to Jonscher's universal power law:[54]

$$\sigma_{AC}(f) = \sigma_t - \sigma_{DC} \approx Af^m \tag{6}$$

where σ_{DC} is the σ_{AC} at $f \to 0$, A is a constant that depends on the temperature, σ_t is the total conductivity, and m is called the exponent of the frequency. Fig. 7(d) illustrates the frequency dependence of σ_{AC} at a constant temperature of 40 °C, the behavior is found a similar even at different temperatures, as seen in Fig. 9 (dielectric properties as functions of temperature at a constant frequency).

Fig. 8 presents ε', ε'' and AC conductivity (σ_{AC}) *versus* frequency (f) at a constant temperature (80 °C). The experimental data of the dielectric constant and electric conductivity of the composites before radiation (Fig. 8a–c) and after effects (Fig. 8d–f) show similar behaviors, indicating that the temperature does not have much effect on the polymeric matrix as a result of the addition of conductive nanoparticles in the PEVA
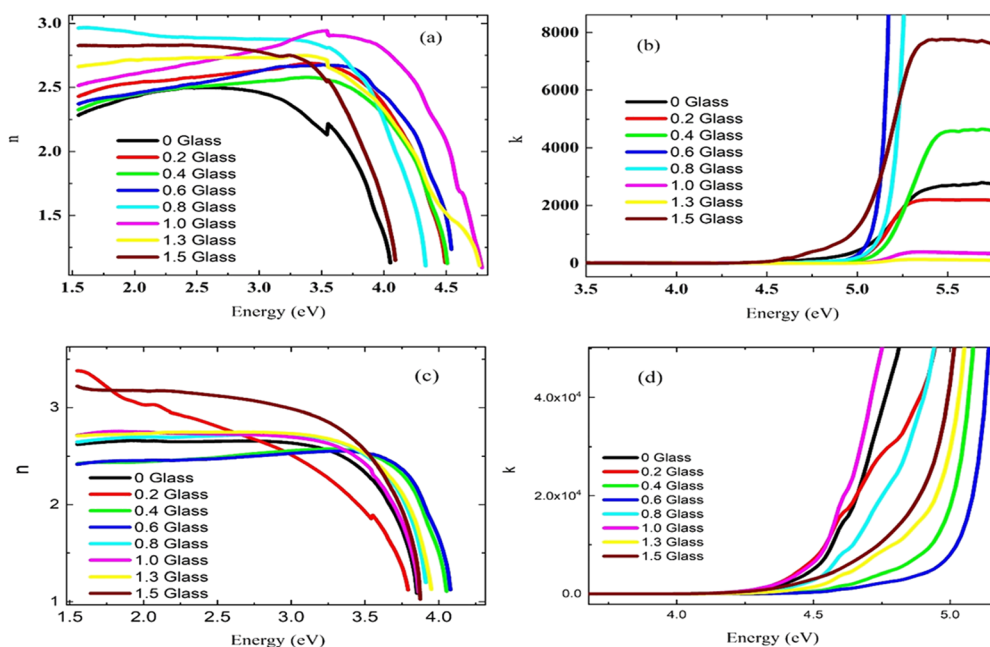
Fig. 6 Refractive indices of the PEVA/glass powder composite membranes with the composition (60% B$_2$O$_3$ − 10% CdO − 15% Na$_2$O − 15% NaF doped with 5% CuO): (a) refractive index and (b) extinction coefficient before irradiation; (c) refractive index and (d) extinction coefficient after irradiation.
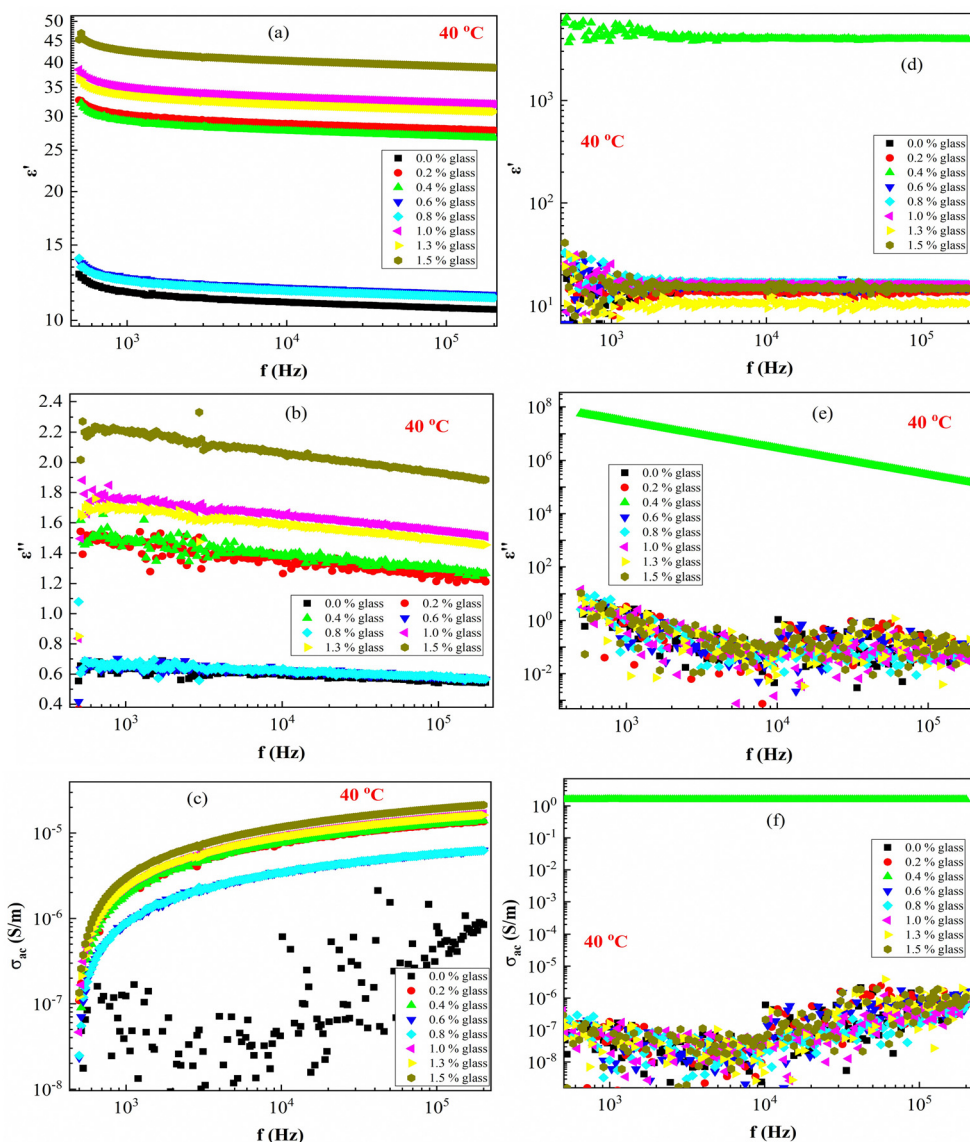
Fig. 7 Dielectric constants (ε' and ε'') and conductivity (σ_{AC}) of PEVA/conductive glass powder composite membranes with the composition (60% B_2O_3 − 10% CdO − 15% Na_2O − 15% NaF doped with 5% CuO) as functions of frequency at a constant temperature (40 °C) (a)−(c) before radiation, and (d)−(f) after radiation.

matrix. The addition of conductive glass to PEVA significantly improves the thermal stability (20 °C to 80 °C) of the composite, as measured experimentally.

As expected, there was a gradual increase in σ_{AC} as the frequency increased. The σ_{AC} curves at various temperatures merged into one single curve at high frequencies ($f > 10^5$ Hz). The conduction might be ascribed to the thermal oscillation-induced tunneling of charge carriers in the PEVA-polymer matrix separating the glass particles. At lower temperatures, conductivity becomes temperature-dependent due to the thermal motion of the conductive glass nanoparticles. This is the typical behavior of nanoparticles combined with a polymer matrix; such behavior has been observed in entirely different types of materials.[55–58] The experimental data of the studied

samples show that ac conductivity increases with increasing frequency and increasing γ-dose radiation, which is similar to the reports of other researchers.[40]

3.5.2. Dielectric properties as functions of temperature. Fig. 9 presents the dielectric constants (ε' and ε'') and conductivity (σ_{AC}) of membranes with the PEVA/glass powder composition (60% B_2O_3 − 10% CdO − 15% Na_2O − 15% NaF doped with 5% CuO) as functions of temperature in the 20–80 °C range at a constant frequency (2 kHz) before and after irradiation. The dielectric constants (ε' and ε'') before irradiation are constant with temperature variation. Further, the dielectric constants of the samples after irradiation decreased except for sample S3 with 0.4% conductive glass content, which showed an increase in ε' values. The behavior of the
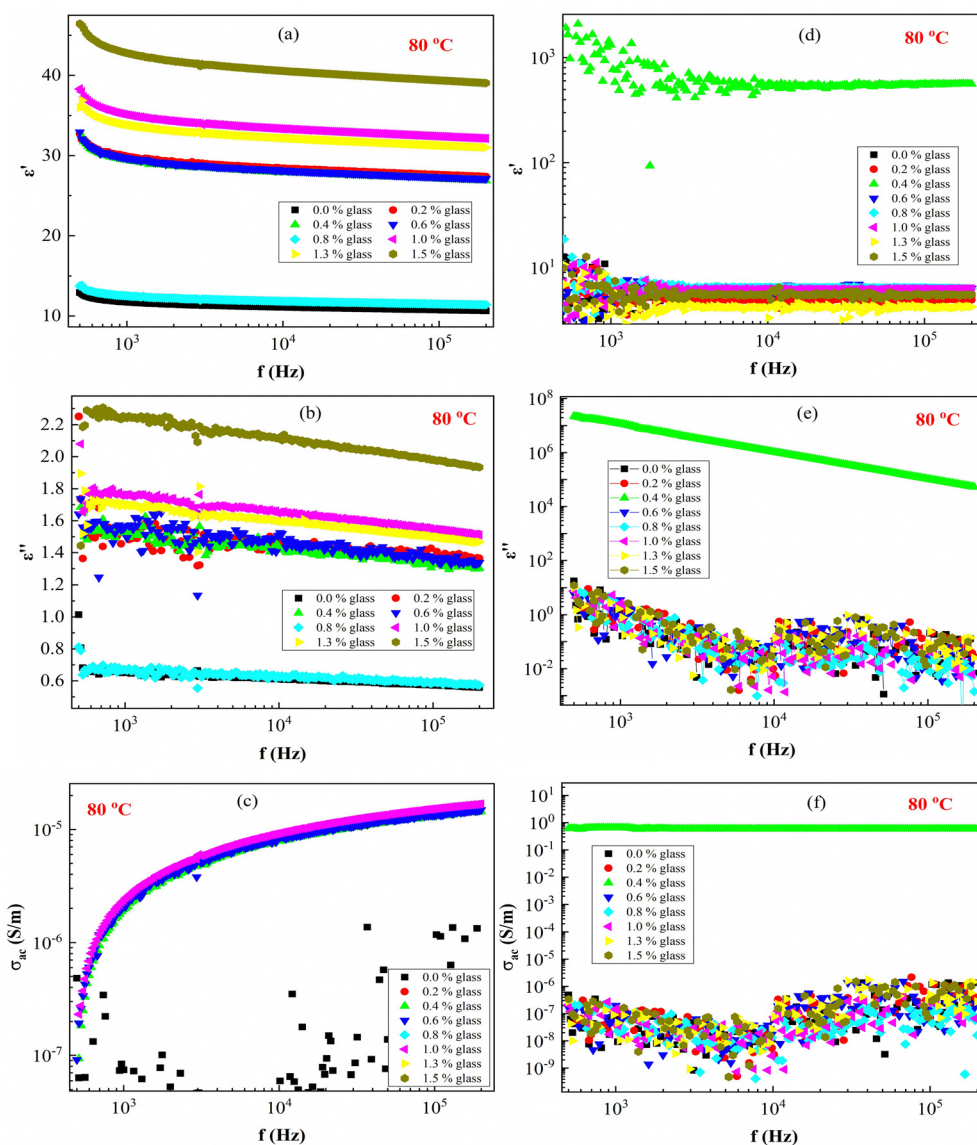
Fig. 8 Dielectric constants (ε' and ε'') and conductivity (σ_{AC}) of composite membranes of PEVA/glass powder composition (60% B_2O_3 − 10% CdO − 15% Na_2O − 15% NaF doped with 5% CuO) as functions of frequency at a constant temperature of 80 °C: (a)−(c) before radiation and (d)−(f) after radiation.

conductivity of all samples remaining constant before irradiation is identical to dielectric behavior. While the effect of radiation on the dielectric constant of sample S3 (0.4) was different from all other samples, the σ_{AC} remained at the same value, with no effect of irradiation. This data means that sample S3 is extremely stable under radiation. Thus, sample S3 can be considered a good candidate for radiation-shielding applications. The addition of conductive glass powder to PEVA improved the thermal stability of the composites in the 20 °C to 80 °C range, as measured experimentally.

4. Conclusions

A series of thin films of poly (ethylene-*co*-vinyl acetate) (PEVA) mixed with different amounts of conductive ground glass powder particles (0, 0.2, 0.4, 0.6, 0.8, 1, 1.3 and 1.5 wt%) was prepared *via* a melt-quenching technique and exposed to irradiation at room temperature in the air. The effects of glass powder concentration and irradiation dose on the electrical and optical properties of the composite sheets were investigated. Moreover, the homogeneity of the dispersion of glass powder in the PEVA matrix was studied based on the crystallinity of the composite sheets through X-ray diffractometry (XRD). Optical studies revealed that the band gap energy decreased with radiation and the content of conductive glass; this may be due to the excitation of electrons from the valence band to the conduction band. When the PEVA polymer with conductive glass additive was exposed to radiation, it demonstrated improved thermal stability and hence can be regarded as a radiation-shielding material candidate for several industrial applications.
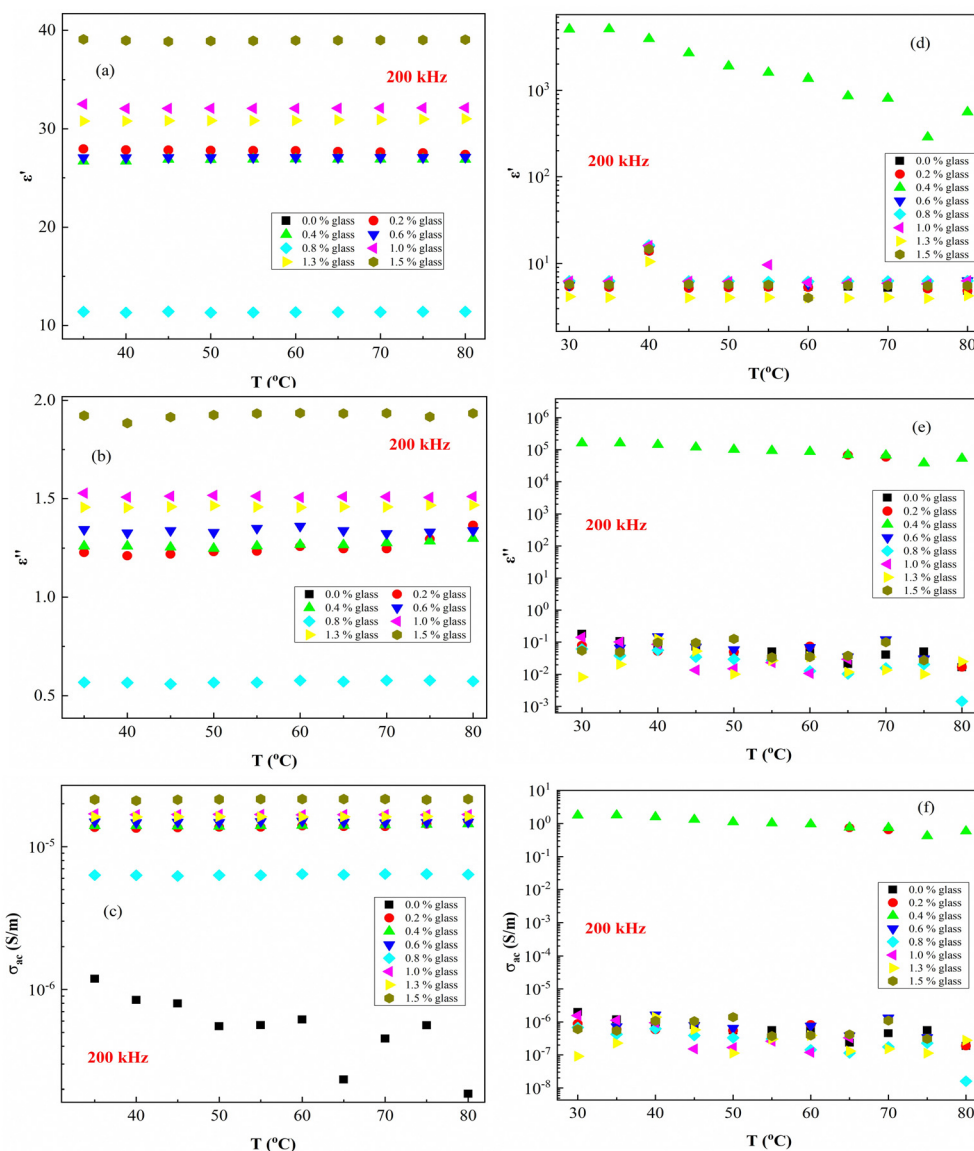
Fig. 9 Dielectric constants (ε' and ε'') and conductivity (σ_{AC}) of composite membranes with PEVA/conductive glass powder composition (60% B_2O_3 – 10% CdO – 15% Na_2O – 15% NaF doped with 5% CuO) as functions of temperature at a fixed frequency of 200 kHz before irradiation (a), (b), and (c) and after irradiation (d), (e), and (f).

Author contributions

O. I. Sallam and Ehab E. Khozemy: experimental part and part of analysis; Mohamed Morsy, Elbadawy A. Kamoun, Ahmed. I. Ali: characterization, data analysis, investigated the experimental results, and wrote and revised the final draft; Galal H. Ramzy: investigated the dielectric properties data, Yasair Al-Faiyez and Saleh M. Matar: data analysis and materials donation; Yeog Son reviewed the manuscript. All authors have critically reviewed and approved the final draft and are responsible for the content and similarity index of the manuscript.

Availability of data and materials

The datasets used and analyzed during the current study are available from the corresponding author on reasonable request.

Conflicts of interest

The authors declare that they have no competing interests.

References

1 N.-Y. Huang, C.-C. Wang and C.-Y. Chen, Gas-permeation properties of sandwich-like polyaniline/poly (ethylene vinyl acetate) nanocomposite membranes, *Chem. Eng. Res. Des.*, 2021, **170**, 239–247.

2 Z. Jiang, *et al.*, Evaluation of physical, rheological, and structural properties of vulcanized EVA/SBS modified bitumen, *J. Appl. Polym. Sci.*, 2017, **134**(21), 44850–44860.

3 R. Dutta, *et al.*, Removal of organic solvents and oils from wastewater by absorption with crosslinked poly (ethylene-*co*-

vinyl acetate) modified by cetyl alcohol, *J. Water Process. Eng.*, 2022, **49**, 103073.

4 S. Kozhabekov, A. Zhubanov and Z. Toktarbay, Study the rheological properties of waxy oil with modified pour point depressants for the South Turgai oil field in Kazakhstan, *Oil Gas Sci. Technol.*, 2019, **74**, 28.

5 M. Giurginca, L. Popa and T. Zaharescu, Thermo-oxidative degradation and radio-processing of ethylene vinyl acetate elastomers, *Polym. Degrad. Stab.*, 2003, **82**(3), 463–466.

6 A. Alsabbagh, *et al.*, Effects of gamma irradiation on 3D-printed polylactic acid (PLA) and high-density polyethylene (HDPE), *Polym. Bull.*, 2021, **78**, 4931–4945.

7 Z. Wang, *et al.*, Porous poly (vinylidene fluoride) supported three-dimensional poly (ethylene glycol) thin solid polymer electrolyte for flexible high temperature all-solid-state lithium metal batteries, *Chem. Eng. J.*, 2022, **435**, 135106.

8 R. Dutta, *et al.*, Removal of Organic Solvents and Oils from Wastewater by Absorption with Crosslinked Poly (Ethylene-Co-Vinyl Acetate) Modified by Cetyl Alcohol. Jour Potash Feldspar Composites, *J. Adv. Res. Mater. Sci.*, 2015, 8–19.

9 A. A. D'souza and R. Shegokar, Polyethylene glycol (PEG): a versatile polymer for pharmaceutical applications, *Expert Opin. Drug Delivery*, 2016, **13**(9), 1257–1275.

10 T. Iqbal, *et al.*, ZnO–PVA polymer matrix with transition metals oxide nano-fillers for high dielectric mediums, *J. Polym. Environ.*, 2020, **28**, 2422–2432.

11 E. Uslu, *et al.*, Determination of mechanical properties of polymer matrix composites reinforced with electrospinning N66, PAN, PVA and PVC nanofibers: A comparative study, *Mater. Today Commun.*, 2021, **26**, 101939.

12 F. La Mantia, *et al.*, A simple method to interpret the rheological behaviour of intercalated polymer nanocomposites, *Composites, Part B*, 2016, **98**, 382–388.

13 S. Choudhary, Structural, morphological, thermal, dielectric, and electrical properties of alumina nanoparticles filled PVA–PVP blend matrix-based polymer nanocomposites, *Polym. Compos.*, 2018, **39**(S3), E1788–E1799.

14 K. Ariane, *et al.*, Effect of P2O5 and Al2O3 on crystallization, structure, microstructure and properties of Li2O–MgO–Al2O3–SiO2–TiO2–ZrO2 glass ceramics, *Bol. Soc. Esp. Ceram. Vidrio*, 2022, **61**(2), 146–159.

15 M. Khalaf, *et al.*, Polyelectrolyte membranes based on phosphorylated-PVA/cellulose acetate for direct methanol fuel cell applications: synthesis, instrumental characterization, and performance testing, *Sci. Rep.*, 2023, **13**(1), 13011.

16 A. M. El Nahrawy, *et al.*, Talented Bi0.5Na0.25K0.25TiO3/oxidized cellulose films for optoelectronic and bioburden of pathogenic microbes, *Carbohydr. Polym.*, 2022, **291**, 119656.

17 A. I. Ali, S. A. Salim and E. A. Kamoun, Novel glass materials-based (PVA/PVP/Al2O3/SiO2) hybrid composite hydrogel membranes for industrial applications: synthesis, characterization, and physical properties, *J. Mater. Sci.: Mater. Electron.*, 2022, **33**(13), 10572–10584.

18 Q. Zhang, L. Wang, L. Wang and C. Zhu, *et al.*, Enhanced Electrochemical Capability of LiNi1/3Co1/3Mn1/3O2 Cathode

Materials Coated with Fluoroborate Glass for Lithium-Ion Batteries, *Chem. Electro. Chem.*, 2017, **4**(5), 1199–1204.

19 K. Wang and Q. Deng, The thermal and mechanical properties of poly (ethylene-co-vinyl acetate) random copolymers (PEVA) and its covalently crosslinked analogues (cPEVA), *Polymers*, 2019, **11**(6), 1055.

20 A. F. Osman, *et al.* Poly (ethylene-co-vinylacetate) copolymer based nanocomposites: A review. in IOP Conference Series: Materials Science and Engineering. 2020. IOP Publishing.

21 N. T.-H. Pham, Characterization of low-density polyethylene and LDPE-based/ethylene-vinyl acetate with medium content of vinyl acetate, *Polymers*, 2021, **13**(14), 2352.

22 O. I. Sallam, N. A. Elalaily, F. M. Ezz-Eldin and A. M. Madbouly, Physical properties and radiation shielding parameters of bismuth borate glasses doped transition metals, *J. Alloys Compd.*, 2020, **843**(30), 156056.

23 I. A. Flora, EPR and magnetic investigations of MnO-B2O3-PbO glasses, *J. Mater. Sci.: Mater. Electron.*, 2002, **13**(6), 357–362.

24 O. I. Sallam, *et al.*, Synthesis and modification of photoluminescence and dielectric properties of novel fluorophosphate glass by incorporating different transition metal oxides for optoelectronic applications, *Opt. Mater.*, 2023, **136**, 113413.

25 H. Adelnia, *et al.*, Permeability and Permselectivity Properties of Ethylene Vinyl Acetate/Sepiolite Mixed Matrix Membranes, *Sep. Purif. Technol.*, 2015, 351–357.

26 O. I. Sallam, A. A.-G. Farrag and N. L. Moussa, Optimizing of optical and structure characters of borate glasses by different concentration of CoO: Electron beam irradiation dosimetry, *Mater. Chem. Phys.*, 2021, **269**(5), 124767.

27 M. Ouis, M. Marzouk and F. ElBatal, Preparation and characterization of glasses from the binary sodium fluoroborate system NaF–B2O3 within the range (10–50 mol% NaF) assessed by structural FTIR, optical and thermal properties and effects of gamma irradiation, *J. Mol. Struct.*, 2022, **1260**, 132881.

28 E. Beyazay, Y. Karabul and S. E. Korkut, Multifunctional PCz/BaO nanocomposites: Ionizing radiation shielding ability and enhanced electric conductivity, *Prog. Nucl. Energy*, 2023, **155**(5–6), 104521.

29 D. D. R. G. Gedam, Impedance spectroscopic characterization of Sm2O3 containing lithium borate glasses, *Spectrochim. Acta, Part A*, 2014, **133**(C), 19–23.

30 N. Mott, Electrons in disordered structures, *Adv. Phys.*, 2001, **50**(7), 865–945.

31 H. Al-Ghamdi, *et al.*, Copper-Doped Borate Glass Systems: Fabrication, Physical and Optical Characteristics, and Efficiency of Radiation Attenuation, *J. Electron. Mater.*, 2023, **52**(12), 7931–7942.

32 T. Naito and R. Doi, Band structure and physical properties of α-STF2I3: Dirac electrons in disordered conduction sheets, *Crystals*, 2020, **10**(4), 270.

33 Z. Jiang, *et al.*, Evaluation of Physical, Rheological, and Structural Properties of Vulcanized EVA/SBS Modified Bitumen, *J. Appl. Polym. Sci.*, 2017, **134**.

34 K. Wa. Q. Deng, The Thermal and Mechanical Properties of Poly(ethylene-co-vinyl acetate) Random Copolymers (PEVA)

and its Covalently Crosslinked Analogues (cPEVA), *Polymers*, 2019, **11**(6), 1055.

35 A. Ali, A. Ammar and A. A. Moez, Influence of substrate temperature on structural, optical properties and dielectric results of nano-ZnO thin films prepared by Radio Frequency technique, *Superlattices Microstruct.*, 2014, **65**, 285–298.

36 G. Demol, T. Paulmier and D. Payan, Analysis of Cathodoluminescence Behavior of Fluoropolymers, *IEEE Trans. Plasma Sci.*, 2023, **51**(9), 2584–2590.

37 A. Ali, *et al.*, Growth and characterization of ZnO: Al thin film using RF sputtering for transparent conducting oxide, *J. Korean Phys. Soc.*, 2006, **49**, S652.

38 J. G. Drobny, *Radiation technology for polymers*, CRC press, 2021.

39 A. I. Ali, H. A. ElMeleegi and A. Abdel Moez, Investigation of structural, optical dielectrical and optical conductivity properties of BaTiO3, Al0.01Ba0.99TiO3 and La0.01Ba0.99TiO3 thin films prepared by pulsed laser deposition, *Phys. Scr.*, 2019, **94**(12), 125810.

40 Y. S. Rammah, S. E. Ibrahim and E. M. Awad, Electrical and optical properties of Makrofol DE 1-1 polymeric films induced by gamma irradiation, *Bull. Natl. Res. Cent.*, 2019, **43**(1), 32.

41 R. A. Elsad, *et al.*, Fabrication, structural, optical, and dielectric properties of PVC-PbO nanocomposites, as well as their gamma-ray shielding capability, *Radiat. Phys. Chem.*, 2021, **189**, 109753.

42 S. C. Sharma and R. A. Ramsey, Effects of gamma radiation on the dielectric and electro-optical properties of a polymer-dispersed liquid crystal, *Phys. B*, 2010, **405**(2), 499–506.

43 M. I. A. Abdel Maksoud, *et al.*, Optical and dielectric properties of polymer nanocomposite based on PVC matrix and Cu/Cu2O nanorods synthesized by gamma irradiation for energy storage applications, *Phys. E*, 2023, **148**, 115661.

44 T. A. Jassim and A. A. Saeed, Effect of Gamma Irradiation on the Physical Properties of PVA Polymer, *IOP Conf. Ser.: Mater. Sci. Eng.*, 2020, **928**(7), 072137.

45 A. M. Abdul-Kader, M. F. Zaki and B. A. El-Badry, Modified the optical and electrical properties of CR-39 by gamma ray irradiation, *J. Radiat. Res. Appl. Sci.*, 2014, **7**(3), 286–291.

46 R. Gerhardt, Impedance and dielectric spectroscopy revisited: Distinguishing localized relaxation from long-range conductivity, *J. Phys. Chem. Solids*, 1994, **55**(12), 1491–1506.

47 A. M. El Nahrawy, *et al.*, Talented Bi0. 5Na0. 25K0. 25TiO3/ oxidized cellulose films for optoelectronic and bioburden of pathogenic microbes, *Carbohydr. Polym.*, 2022, **291**, 119656.

48 M. M. Abdel-Kader, M. Fadly, M. Abu Taleb, K. Eldehamy and A. I. Ali, Electrical conductivity and relative permittivity of KHCO3, *Phys. Status Solidi*, 1994, **142**(1), 69–74.

49 I. S. Elashmawi, *et al.*, Modification and development of electrical and magnetic properties of PVA/PEO incorporated with MnCl2, *Phys. B*, 2014, **434**, 57–63.

50 B. Nageswara Rao, M. Venkateswarlu and N. Satyanarayana, Electrical and dielectric properties of rare earth oxides coated LiCoO2 particles, *Ionics*, 2014, **20**(2), 175–181.

51 F. V. Pranvera Dhima, Polypropylene as a Promising Plastic, *Adv. Mater. Phys. Chem.*, 2018, **8**(6), 1–11.

52 C. Rayssi, S. El-Kossi, J. Dhahri and K. Khirounib, Frequency and temperature-dependence of dielectric permittivity and electric modulus studies of the solid solution Ca0.85Er0.1Ti1−xCo4x/ 3O3 (0 ≤ x ≤ 0.1), *RSC Adv.*, 2018, **8**, 17139–17150.

53 C. Rayssi, *et al.*, Frequency and temperature-dependence of dielectric permittivity and electric modulus studies of the solid solution Ca0.85Er0.1Ti1−xCo4x/3O3 (0 ≤ x ≤ 0.1), *RSC Adv.*, 2018, **8**(31), 17139–17150.

54 R. Singh, *et al.*, Ion-transport behavior in tetraethylene glycol dimethyl ether incorporated sodium ion conducting polymer gel electrolyte membranes intended for sodium battery application, *J. Mol. Liq.*, 2021, **336**, 116594.

55 M. T. Connor, *et al.*, Broadband ac conductivity of conductor-polymer composites, *Phys. Rev. B: Condens. Matter Mater. Phys.*, 1998, **57**(4), 2286.

56 A. Papathanassiou, I. Sakellis and J. Grammatikakis, Universal frequency-dependent ac conductivity of conducting polymer networks, *Appl. Phys. Lett.*, 2007, **91**(12), 122911.

57 C. Tsonos, Comments on frequency dependent AC conductivity in polymeric materials at low frequency regime, *Curr. Appl. Phys.*, 2019, **19**(4), 491–497.

58 G. Psarras, E. Manolakaki and G. Tsangaris, Dielectric dispersion and ac conductivity in—Iron particles loaded---polymer composites, *Composites, Part A*, 2003, **34**(12), 1187–1198.